Multijet production at the LHC: Event shapes, NNLO predictions and α_s

Javier Llorente

CIEMAT

June 29, 2023

Outline of the talk

- Introduction and historical perspective.
  - QCD and running coupling constant $\alpha_s(Q)$.
  - Jets and event shapes in e^+e^-.
  - Fixed order theoretical predictions.
  - Non-perturbative QCD: PDFs and fragmentation.
- The ATLAS detector and jet reconstruction.
  - The ATLAS tracking and calorimeter systems.
  - The Particle Flow algorithm and jet calibration.
  - The jet production cross section.
- ATLAS event shapes and theoretical predictions.
  - Event selection and phase-space definition.
  - Unfolding and systematic uncertainties.
  - Comparison to NNLO predictions.
- TEEC and determination of α_s.
  - Event selection and phase-space definition.
  - Unfolding and systematic uncertainties.
  - Comparison to NNLO predictions.
  - χ^2 fits, α_s and asymptotic freedom.
- Constraining new physics from $\alpha_s(Q)$.

QCD and the running coupling constant

- QCD is the theory of strong interactions between constituents of matter.
- Fermions Ψ_i are known as quarks. Bosons $G^a_\mu(x)$ are known as gluons.

QCD Lagrangian: $\mathcal{L} = -\frac{1}{4} F^a_{\mu\nu} F^{\mu\nu}_a + \sum_{j,k} \bar{\Psi}_j \left(i\gamma^\mu D_\mu - m \right)_{jk} \Psi_k,$ where

- $D_\mu = \partial_\mu - i g_s G^a_\mu(x) \lambda_a$ covariant derivative $\Rightarrow$ quark-gluon interactions.
- $F_{\mu\nu} = \frac{i}{g_s}[D_\mu, D_\nu]$ field strength tensor $\Rightarrow$ gluon-gluon interactions.
- $\alpha_s = \frac{g_s^2}{4\pi}$ is the fundamental parameter of the theory.

Cross sections in QCD can be written as a perturbative expansion on α_s:

$$\frac{d^n\sigma}{d\xi_1 \cdots d\xi_n} = \sum_{k=1}^{\infty} A_k(\xi_1, ..., \xi_n) \left[\frac{\alpha_s(Q^2)}{\pi} \right]^k$$

See [G. P. Salam arXiv:1011.5131] for a nice review

QCD and the running coupling constant

- α_s depends on the interaction scale Q^2 through the RGE:

$$\frac{\partial \alpha_s}{\partial \log Q^2} = \beta(\alpha_s) = -\alpha_s^2(\beta_0 + \beta_1 \alpha_s + \beta_2 \alpha_s^2 + \mathcal{O}(\alpha_s^3))$$

- The solution at three-loop precision reads

$$\frac{\alpha_s}{4\pi}(Q^2) = \frac{1}{\beta_0 x}\left[1 - \frac{\beta_1}{\beta_0^2}\frac{\log x}{x} + \frac{\beta_1^2}{\beta_0^4 x^2}\left(\log^2 x - \log x - 1 + \frac{\beta_2 \beta_0}{\beta_1^2}\right)\right]; \quad x = \log\left(\frac{Q^2}{\Lambda^2}\right)$$

Standard Model with n_f quark flavours:

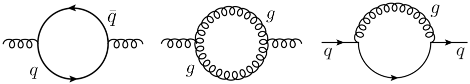

$$\left.\begin{aligned} \beta_0 &= 11 - \frac{2}{3} n_f \\ \beta_1 &= 102 - \frac{38}{3} n_f \\ \beta_2 &= \frac{2857}{2} - \frac{5033}{18} n_f - \frac{325}{54} n_f^2 \end{aligned}\right\}$$

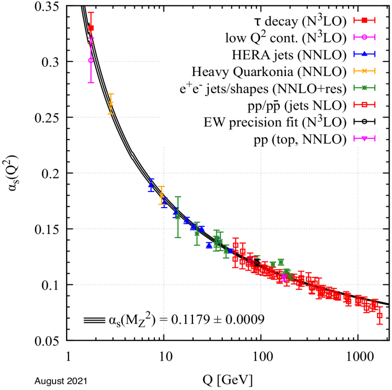

[Prog. Theor. Exp. Phys. 083C01 (2022)]

Jets and the anti-k_t algorithm

- Jets are collimated sprays of hadrons from the hadronisation of partons.
- Aim to fully contain the shower from the parton cascade: $\vec{p}_p \sim \sum_h \vec{p}_h$.
- Jets can be reconstructed using iterative algorithms: k_t, anti-k_t, C/A, ...
- Algorithm seeded by jet constituents: partons, hadrons or detector objects.

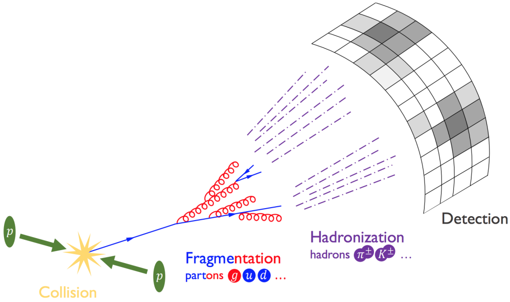

Courtesy of E. Metodiev

anti-k_t algorithm [JHEP 04 (2008) 063]

$$\left.\begin{aligned} d_{ij} &= \min\left(\frac{1}{k_{Ti}^2}, \frac{1}{k_{Tj}^2}\right)\frac{\Delta R_{ij}^2}{R^2} \\ d_{iB} &= \frac{1}{k_{Ti}^2} \end{aligned}\right\}$$

- Find $\min_j \{d_{ij}, d_{iB}\}$ for constituent i.
- If it's d_{ij}, combine constituents i, j.
- If it's d_{iB}, call i a jet.
- Iterate until no constituents left.

Global event structure: event shapes in e^+e^- annihilation.

- Experimentally, three-jet production is an ideal playground to measure α_s.
- Event shapes: Observables quantifying the isotropy of energy distribution.
- Historically, event shapes were developed for $e^+e^- \rightarrow q\bar{q}(g)$ annihilation.
- A classic example is Thrust [ALEPH Coll., Eur. Phys. J. C 35 457 (2004)].

$$T = \max_{|\vec{n}|=1} \frac{\sum_i |\vec{n}\cdot\vec{p}_i|}{\sum_i |\vec{p}_i|} \Rightarrow \begin{cases} T \rightarrow 1 : \text{Pencil-like event} \\ T \rightarrow \frac{2}{3} : \text{Isotropic event} \end{cases}$$

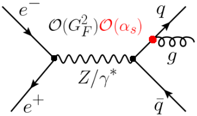

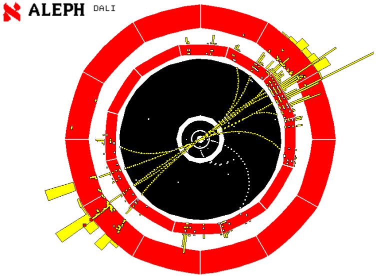

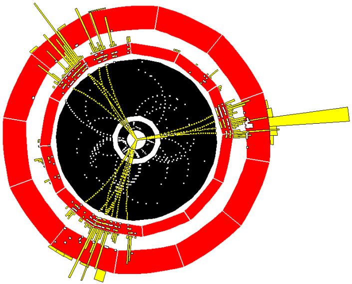

Fixed order theoretical predictions to three-jet production

- Back to the LHC, high-accuracy predictions needed to compare to data.
- The QCD cross section can be factorised [PDF $\otimes$ Matrix element $\otimes$ Frag.]

$$d\sigma_3 = \sum_{i,j,a,b,c} \int_\Omega d^2\vec{x} d^3\vec{z}\, f_i(x_1, \mu_F^2) f_j(x_2, \mu_F^2) d\hat{\sigma}_{ij\to abc}(\vec{x}, \mu_R^2) D_a^h(z_3, \mu_f^2) D_b^h(z_4, \mu_f^2) D_c^h(z_5, \mu_f^2)$$

LO

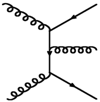

Born $\mathcal{O}(\alpha_s^3)$

$$\hat{\sigma}_{ij\to abc} \propto |\mathcal{M}|^2 = \sum_{i,j\in\mathcal{D}} \mathcal{M}_i^* \mathcal{M}_j$$

PDFs from LHAPDF [EPJC 75, 132 (2015)]

NLO

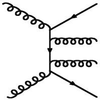

Real finite $\mathcal{O}(\alpha_s^4)$

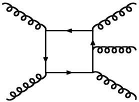

Virtual finite $\mathcal{O}(\alpha_s^5)$

Fragmentation from MC
[2203.11601], [1512.01178]

NNLO

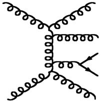

Real-real finite $\mathcal{O}(\alpha_s^5)$

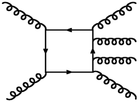

Real-virtual finite $\mathcal{O}(\alpha_s^6)$

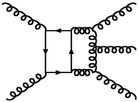

Virtual-virtual finite $\mathcal{O}(\alpha_s^7)$.

- Probability $f_i(x, Q)$ of parton i carrying momentum fraction x at scale Q.
- Need to be obtained from fits to DIS ($+pp$ @ LHC) data.
- Different sets available, depending on fitted datasets, parameterisation, ...

See [ATLAS Collaboration EPJC 82, 438 (2022)] and references therein

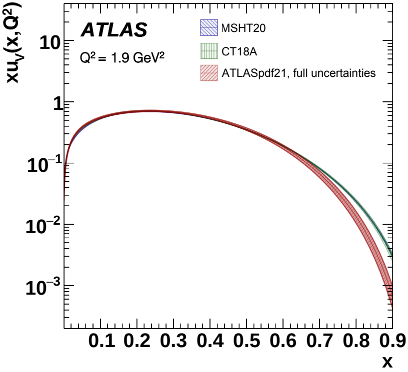

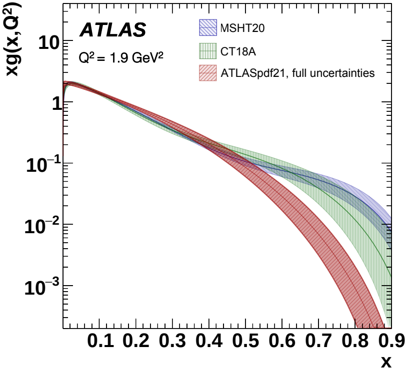

Different parameterisations can differ substantially at high-x!

Parton shower Monte Carlo predictions

- Attempt to simulate all aspects of collisions.
- Matrix elements calculated at fixed order.
- Parton showers simulate all-order emissions.
- Simulates non-pert. hadron fragmentation.
  - Lund string hadronization ⇒ Pythia 8.
  - Cluster hadronization ⇒ Herwig 7.
- Underlying event from multiparton interactions

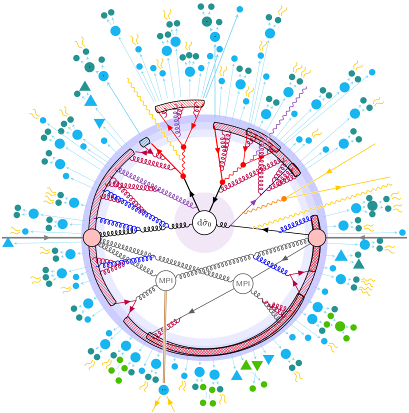

○ Hard Interaction
● Resonance Decays
■ MECs, Matching & Merging
■ FSR
■ ISR*
■ QED
■ Weak Showers
○ Multiparton Interactions

Generator	ME order	FS partons	PDF set	Parton shower	Scales μ_R, μ_F	$\alpha_s(m_Z)$
Pythia	LO	2	NNPDF 2.3 LO	p_T-ordered	$(m_{T3} \cdot m_{T4})^{\frac{1}{2}}$	0.140
Sherpa	LO	2,3	CT14 NNLO	CSS (dipole)	$H(s,t,u)$ [2 → 2] CMW [2 → 3]	0.118
MG5_aMC	LO	2,3,4	NNPDF 3.0 NLO	p_T-ordered	m_T	0.118
Herwig	NLO	2,3	MMHT2014 NLO	Angle-ordered Dipole	$\max_i \{p_{Ti}\}_{i=1}^{N}$	0.120

Parton shower Monte Carlo predictions

- How well do Monte Carlo predictions work?
- MC models validated against a huge variety of data
- Non-pQCD effects (frag, UE) reasonably well described.
- Fragmentation: Measurement of $\zeta = p_T^{\rm ch}/p_T^{\rm jet}$ in jets.
- UE: Measurement of $\langle p_T \rangle$ in transverse regions.

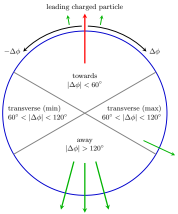

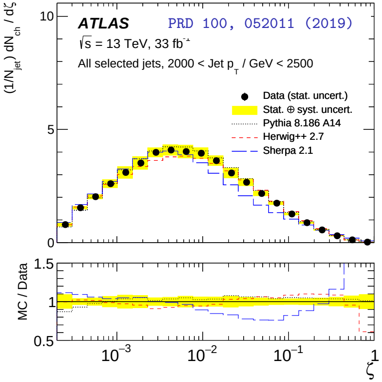

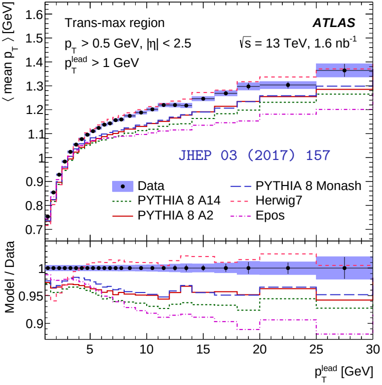

The ATLAS Tracking System

- Innermost part of the ATLAS detector, containing three subdetectors.
  - Four layers of Silicon pixel detectors (PIX).
  - Four layers of Silicon microstrip detectors (SCT).
  - A transition radiation tracker made of gaseous straws (TRT).
- High efficiency reconstruction of charged particles ($\pi^{\pm}, K^{\pm}, \mu^{\pm}, e^{\pm}, ...$).
- Excellent momentum and spatial resolution for charged particle tracks.

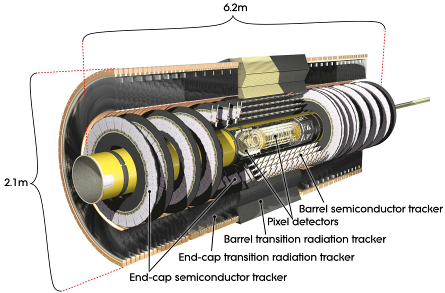

$B^{\pm} \to J/\psi K^{\pm}$ reconstruction

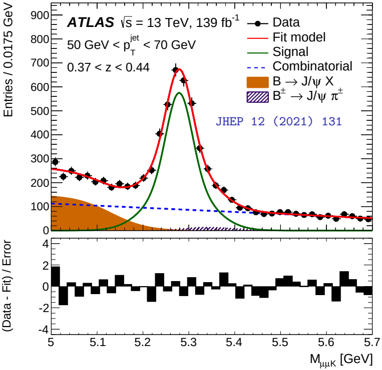

- Contains two subsystems: Electromagnetic (ECAL) and Hadronic (HCAL)
- ECAL composed of Liquid Argon and electrodes $\Rightarrow e^{\pm}, \gamma$ reconstruction.
- Tile Hadronic calorimeter composed of steel and scintillator material.
- Hadronic endcaps (forward rapidity) composed of Liquid Argon.
- Energy deposits form clusters of cells using an iterative algorithm.

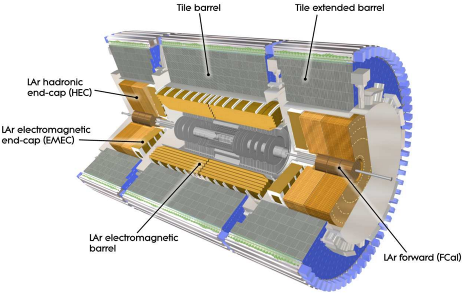

$H \to \gamma\gamma$ reconstruction

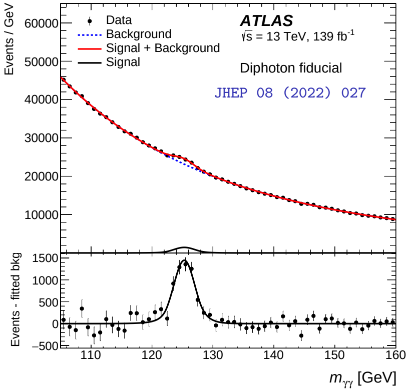

- Jets contain both neutral and charged hadrons $(\pi^0, \pi^\pm, ...)$.
- Tracking has much better spatial and $|\vec{p}|$-resolution than calorimeter.
- Use track information when available, use calo info for neutrals (PFO).
- Jets are built from PFO inputs, then follow a calibration procedure.
- Uncertainty on jet p_T derived using in situ methods ranging $\mathcal{O}(1-5\%)$.

[Eur. Phys. J. C 77, 466 (2017)]

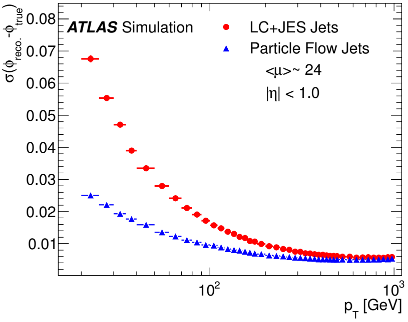

[Eur. Phys. J. C 81, 689 (2021)]

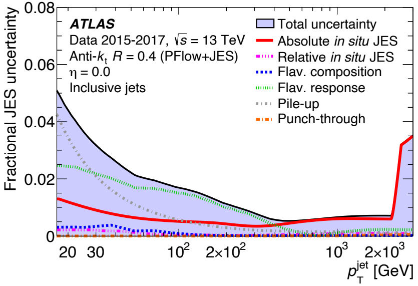

The jet production cross section [JHEP 05 (2018) 195]

- Jet production cross section falls steeply as a function of jet p_T and m_{jj}.
- NLO QCD, with NP and EW corrections, gives a reasonable description.
- Probes different p_T scales, from 100 GeV to 4 TeV, for various y bins.
- Comparison to NLO and NNLO predictions with different scale choices.

$$\text{Inclusive: } \frac{d^2\sigma}{dp_T dy}; \quad \text{Dijets: } \frac{d^2\sigma}{dm_{jj}dy^*} \text{ with } y^* = \frac{1}{2}|y_1 - y_2|$$

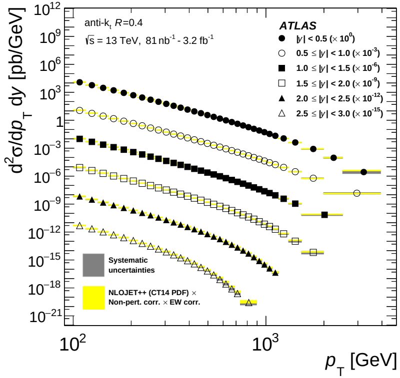

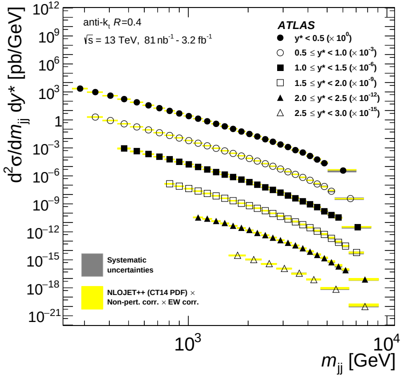

The jet production cross section [JHEP 05 (2018) 195]

- PDF uncertainties increase with jet p_T (high x!)
- Scale uncertainties on μ_R, μ_F dominant.
- Important dependence on $\mu = p_T^{\max}$ vs. $\mu = p_T^{\text{jet}}$.
- Difference treated as an additional uncertainty.

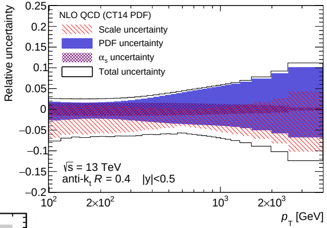

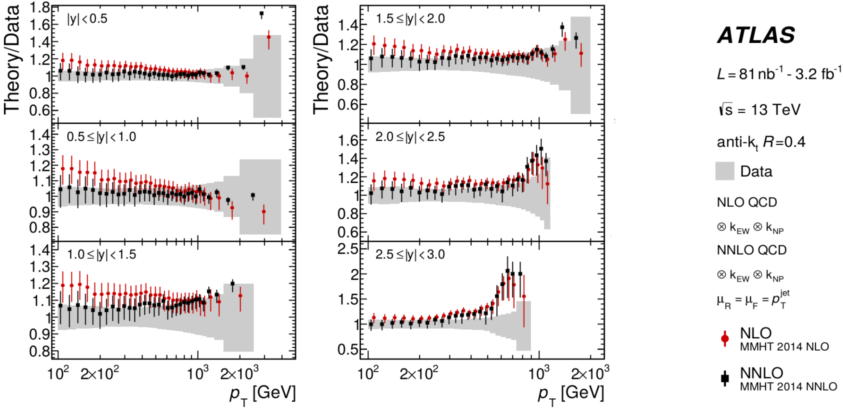

- Event shapes characterise the isotropy of the energy distribution.
- Two main families are considered: Thrust-based and Sphericity-based.
- Transverse Thrust and Transverse Thrust Minor:

$$\tau_\perp = 1 - \frac{\sum_i |\vec{p}_{\mathrm{T},i} \cdot \hat{n}_{\mathrm{T}}|}{\sum_i |\vec{p}_{\mathrm{T},i}|}; \qquad T_\mathrm{m} = \frac{\sum_i |\vec{p}_{\mathrm{T},i} \times \hat{n}_{\mathrm{T}}|}{\sum_i |\vec{p}_{\mathrm{T},i}|}$$

- The 2 and 3-dimensional Sphericity tensors $\mathcal{M}_{\alpha\beta} = \frac{1}{\sum_i |\vec{p}_i|} \sum_i \frac{p_i^\alpha p_i^\beta}{|\vec{p}_i|}$, i.e.

$$\mathcal{M}_2 = \frac{1}{\sum_i |\vec{p}_i|} \sum_i \frac{1}{|\vec{p}_i|} \begin{pmatrix} p_{\mathrm{x}i}^2 & p_{\mathrm{x}i} p_{\mathrm{y}i} \\ p_{\mathrm{y}i} p_{\mathrm{x}i} & p_{\mathrm{y}i}^2 \end{pmatrix}$$

$$\mathcal{M}_3 = \frac{1}{\sum_i |\vec{p}_i|} \sum_i \frac{1}{|\vec{p}_i|} \begin{pmatrix} p_{\mathrm{x}i}^2 & p_{\mathrm{x}i} p_{\mathrm{y}i} & p_{\mathrm{x}i} p_{\mathrm{z}i} \\ p_{\mathrm{y}i} p_{\mathrm{x}i} & p_{\mathrm{y}i}^2 & p_{\mathrm{y}i} p_{\mathrm{z}i} \\ p_{\mathrm{z}i} p_{\mathrm{x}i} & p_{\mathrm{z}i} p_{\mathrm{y}i} & p_{\mathrm{z}i}^2 \end{pmatrix}$$

Eigenvalues $\mu_i \in \sigma(\mathcal{M}_2)$ and $\lambda_i \in \sigma(\mathcal{M}_3)$

$$\mu_1 \geq \mu_2; \quad \lambda_1 \geq \lambda_2 \geq \lambda_3$$

- Transverse Sphericity $S_\perp = \frac{2\mu_2}{\mu_1+\mu_2}$
- Aplanarity $A = \frac{3}{2}\lambda_3$
- $C = 3(\lambda_1\lambda_2 + \lambda_1\lambda_3 + \lambda_2\lambda_3)$
- $D = 27\lambda_1\lambda_2\lambda_3$

Measurement of event shapes in ATLAS [JHEP 01 (2021) 188]

- Jets are built with anti-k_t, $R = 0.4$ from Particle Flow objects.
- Jets with $p_T > 100$ GeV and $|\eta| < 2.4$ are preselected.
- Events with at least two jets with $H_{T2} = p_{T1} + p_{T2} > 1$ TeV.
- Three H_{T2} regions are considered $\mathcal{R} = \{1.0\text{ TeV},\ 1.5\text{ TeV},\ 2.0\text{ TeV}, \sqrt{s}\}$.

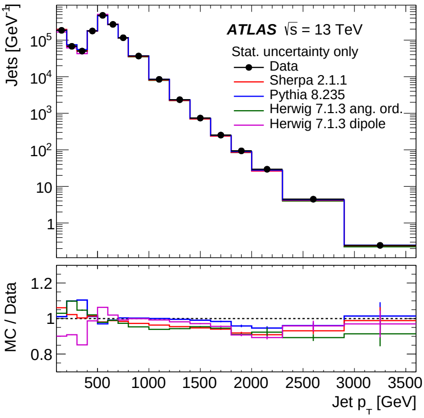

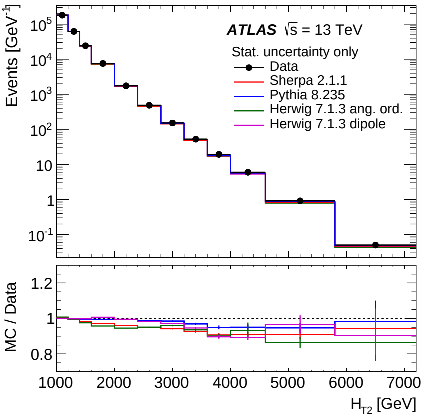

- Event-shape distributions obtained at detector level versus H_{T2} and n_{jet}.
- Distributions to be corrected for detector effects (resolution, efficiency, ...)
- Need to take into account migrations between (H_{T2}, n_{jet}) bins.
- This is achieved by solving a linear problem in $\tau_{\perp} \otimes H_{T2} \otimes n_{\text{jet}}$ dimensions.

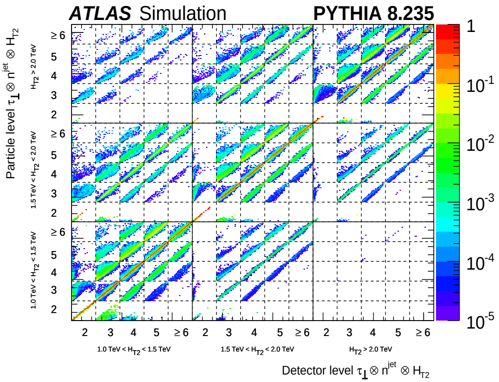

$$R_i = \sum_j \frac{\mathcal{E}_j}{\mathcal{P}_i} M_{ij} T_j$$

- R_i is the detector-level distribution.
- $\mathcal{E}_j$ is the reconstruction efficiency.
- $\mathcal{P}_i$ is the reconstruction purity.
- M_{ij} is the transfer matrix.
- T_j is the particle-level distribution.

- Systematic uncertainties on jet energy (JES, JER) are dominant.
- Unfolding is performed with different Monte Carlo models.
- Jet Angular Resolution and Pileup are subdominant.
- Uncertainties range from $\mathcal{O}(1\%)$ to $\mathcal{O}(7\%)$ with increasing jet multiplicity.

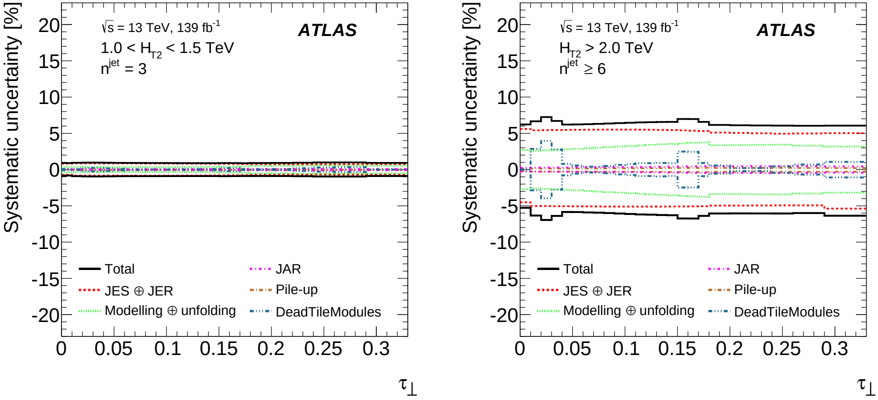

- After unfolding, the multijet cross section is presented versus n_{jet}.
- Results compared to different MC models (Pythia, MG5, Herwig, Sherpa).
- A reasonable description is obtained up to exclusive three-jets bin.
- Important (expected) differences observed among MC models for $n_{\mathrm{jet}} \geq 4$.

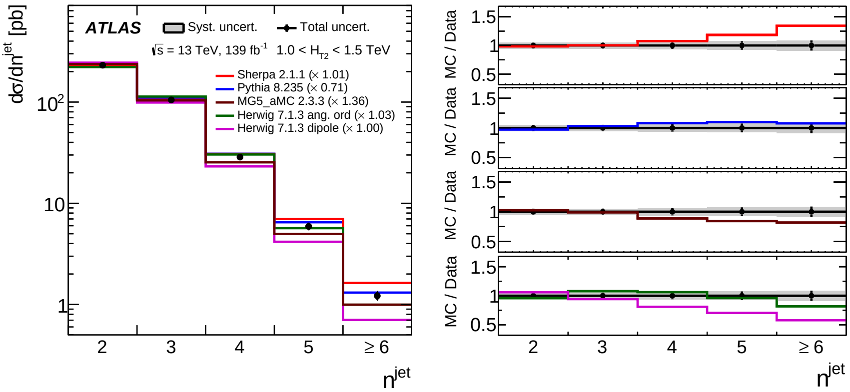

- For each bin, the distributions are normalised to two-jet cross section σ_2.
- Large jet multiplicities implies more isotropic events.
- No MC model fully describes the data, either in shape or normalisation.
- As expected the description is worse for larger jet multiplicities.

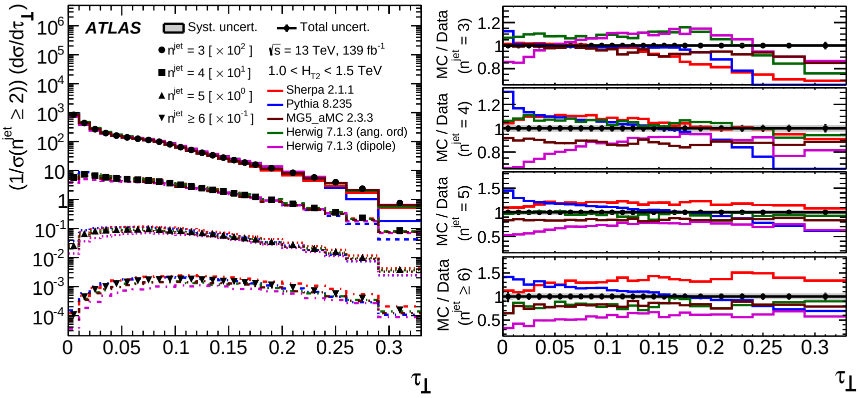

- For each bin, the distributions are normalised to two-jet cross section σ_2.
- Large jet multiplicities implies less planar events.
- No MC model fully describes the data, either in shape or normalisation.
- As expected the description is worse for larger jet multiplicities.

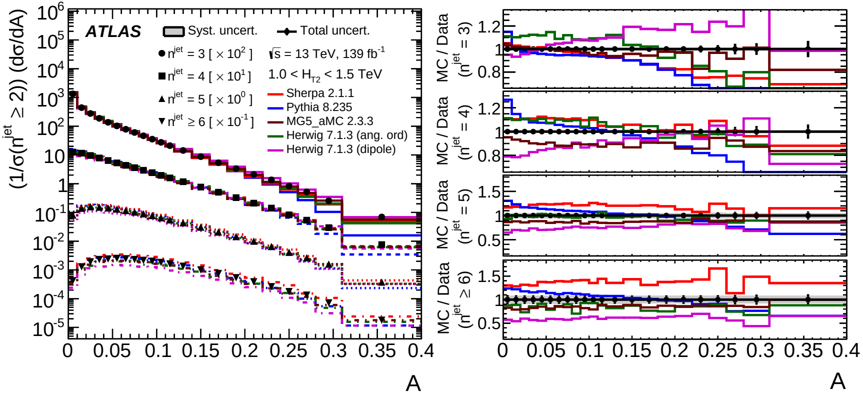

NNLO QCD corrections to event shapes [JHEP 03 (2023) 129]

- Perturbative QCD can be used to calculate predictions to event shapes.
- Calculation needs to estimate integrated σ_2 and differential σ_3 separately.
- To ensure good cancellations, predictions calculated for inclusive 3-jet bins.

$$\left(\frac{d\sigma_3}{dH_{T2}dx}\right)_{n_j\geq 3} = \left(\frac{d\sigma_3}{dH_{T2}dx}\right)_{n_j=3} + \left(\frac{d\sigma_3}{dH_{T2}dx}\right)_{n_j=4} + \left(\frac{d\sigma_3}{dH_{T2}dx}\right)_{n_j=5} + \left(\frac{d\sigma_3}{dH_{T2}dx}\right)_{n_j\geq 6}$$

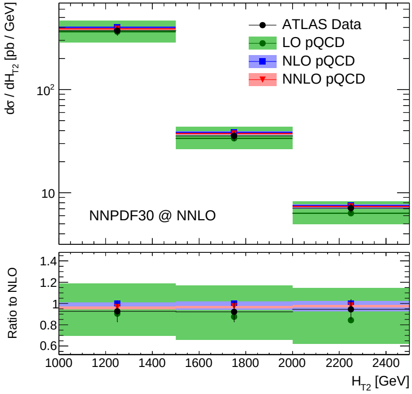

- Scale choice $\mu_R = \mu_F = \hat{H}_T = \sum_{\text{partons}} p_{Ti}$
- Different PDF parameterisations are used:
  - NNPDF 3.0 [JHEP 04 (2015) 040]
  - MMHT 2014 [EPJC 75, 204 (2015)]
  - CT18 [PRD 103, 014013 (2021)]
  - HERAPDF 2.0 [EPJC 75, 580 (2015)]
- Central predictions slightly overestimate dijet cross sections.
- Good agreement within experimental and theoretical uncertainties.

NNLO QCD corrections to event shapes [JHEP 03 (2023) 129]

- Non-pQCD corrections cover jet fragmentation and UE effects.
- The effect of these corrections is limited to $\mathcal{O}(1\%)$ in all regions.
- They are estimated using different MC models and tunes as the ratio

$$C_{NP} = \left(\frac{1}{\sigma_2}\frac{d\sigma_3}{dX}\right)^{\mathrm{Had=ON}}_{\mathrm{UE=ON}} \Bigg/ \left(\frac{1}{\sigma_2}\frac{d\sigma_3}{dX}\right)^{\mathrm{Had=OFF}}_{\mathrm{UE=OFF}} \quad ; \quad X = \tau_\perp, T_m, A, \ldots$$

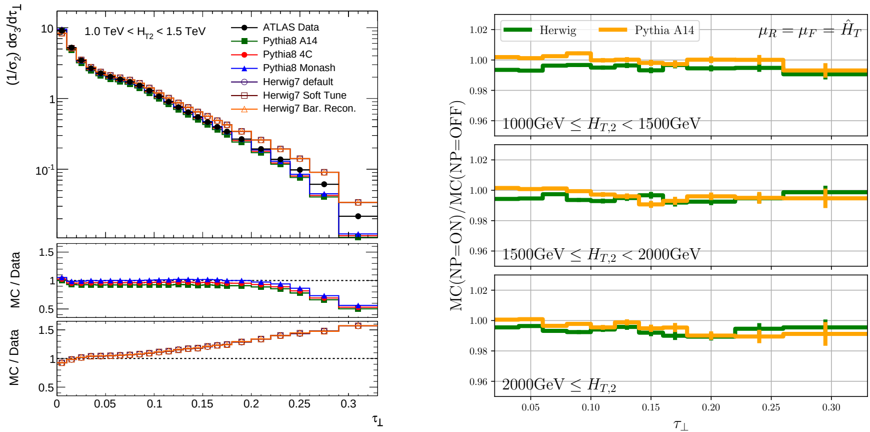

NNLO QCD corrections to event shapes [JHEP 03 (2023) 129]

- Each additional perturbative order adds for a better description of $\tau_\perp$.
- Scale uncertainties reduce with each additional perturbative order.
- NNLO predictions describe the data well, specially for high $\tau_\perp$.
- Low values of $\tau_\perp$ can be subject to additional resummed corrections.

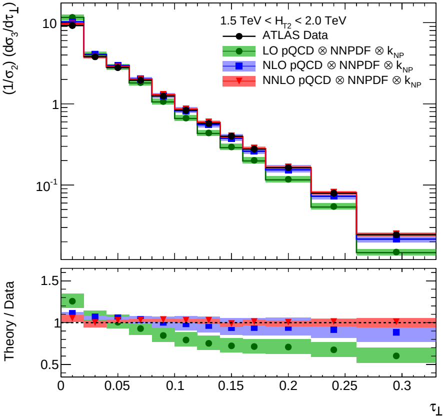

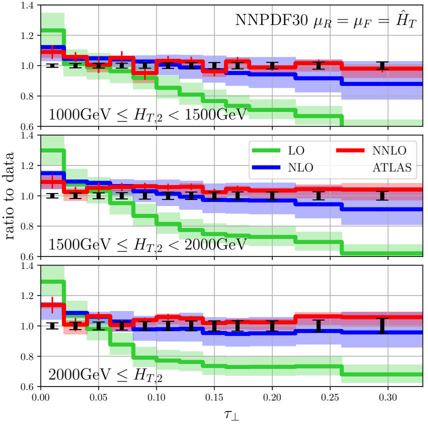

NNLO QCD corrections to event shapes [JHEP 03 (2023) 129]

- Each additional perturbative order adds for a better description of A.
- Scale uncertainties reduce with each additional perturbative order.
- NNLO predictions describe the data well, specially for high A.
- Low values of A can be subject to additional resummed corrections.

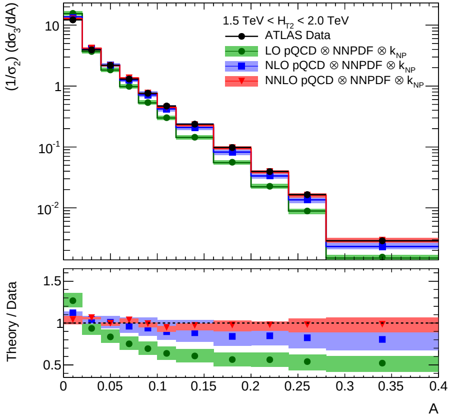

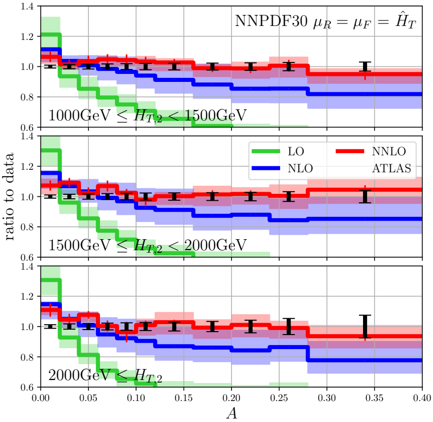

NNLO QCD corrections to event shapes [JHEP 03 (2023) 129]

- The differences between PDF sets is studied for each observable.
- In general, a good compatibility is observed within PDF uncertainties.
- HERAPDF 2.0 shows the largest differences with respect to the others.

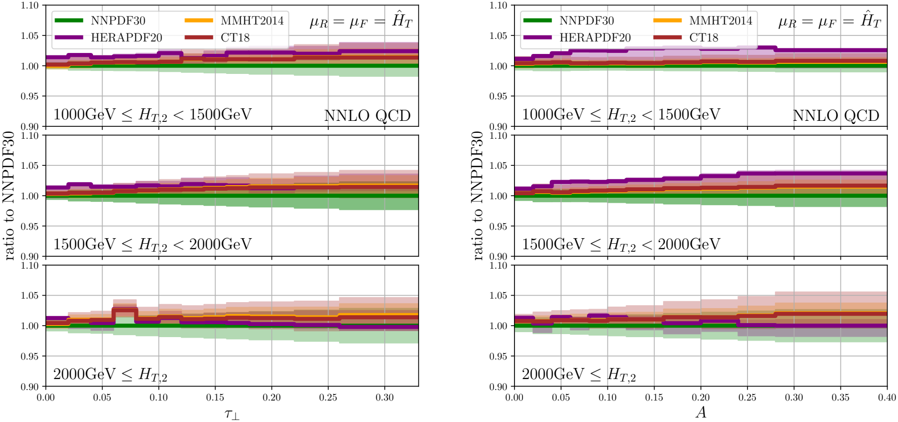

- α_s-dependence estimated using variations provided by each PDF group.
- Considering the Taylor expansion around $\alpha_{s,0} = 0.1180$:

$$R_{NNLO}(\alpha_s) = \sum_{k=0}^{\infty} c_k(\alpha_s - \alpha_{s,0})^k \quad \text{with } c_k = \left.\frac{\partial^k R}{\partial \alpha_s^k}\right|_{\alpha_s=\alpha_{s,0}}$$

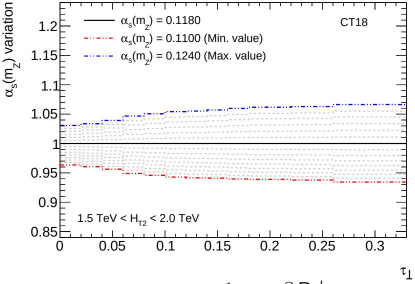

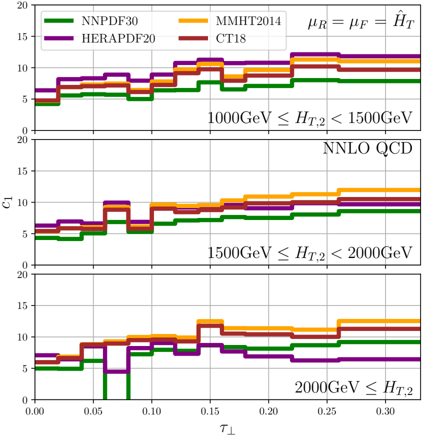

$$\text{Let } \tilde{c}_1 = \frac{c_1}{c_0} = \frac{1}{R(\alpha_{s,0})} \left.\frac{\partial R}{\partial \alpha_s}\right|_{\alpha_s=\alpha_{s,0}}$$

- Larger dependence observed for high $\tau_\perp$.
- Slight dependence on PDF choice for $\tilde{c}_1$.

TEEC: The x_{T}-weighted distribution of differences in azimuth between jets i and j, with $x_{\mathrm{T}i} = \frac{E_{\mathrm{T}i}}{\sum_k E_{\mathrm{T}k}}$

$$\frac{1}{\sigma}\frac{d\Sigma}{d(\cos\phi)} = \frac{1}{\sigma}\sum_{ij}\int \frac{d\sigma}{dx_{\mathrm{T}i}dx_{\mathrm{T}j}d(\cos\phi)} x_{\mathrm{T}i}x_{\mathrm{T}j}dx_{\mathrm{T}i}dx_{\mathrm{T}j}$$

And the azimuthal asymmetry ATEEC is defined as

$$\frac{1}{\sigma}\frac{d\Sigma^{\mathrm{asym}}}{d(\cos\phi)} \equiv \frac{1}{\sigma}\frac{d\Sigma}{d(\cos\phi)}\bigg|_{\phi} - \frac{1}{\sigma}\frac{d\Sigma}{d(\cos\phi)}\bigg|_{\pi-\phi}$$

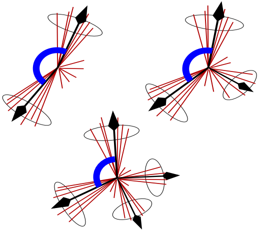

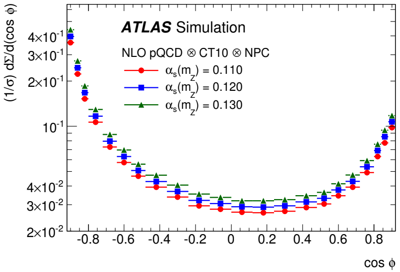

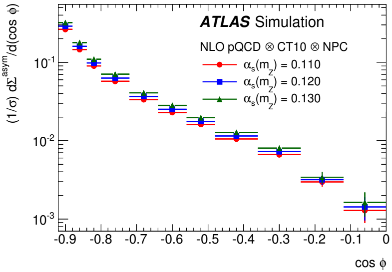

ATLAS Collaboration, [Phys. Lett. B 750,427 (2015)], [Eur. Phys. J. C 77, 872 (2017)]

- Small sensitivity to IR divergences and mild dependence on PDF and μ_R, μ_F.
- Good stability against JES and JER due to $x_{\mathrm{T}i}x_{\mathrm{T}j}$-weighting

- Jets are built with anti-k_t, $R = 0.4$ from Particle Flow objects.
- Jets with $p_T > 60$ GeV and $|\eta| < 2.4$ are preselected.
- Events with at least two jets with $H_{T2} = p_{T1} + p_{T2} > 1$ TeV.
- Ten H_{T2} regions are considered, from 1.0 up to 3.5 TeV.

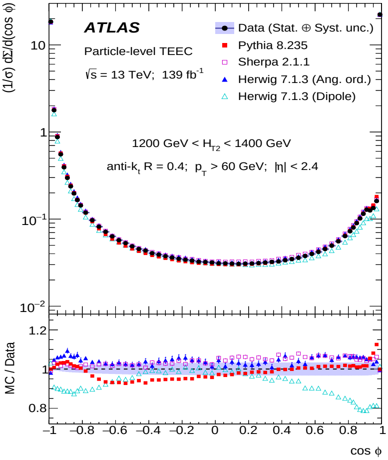

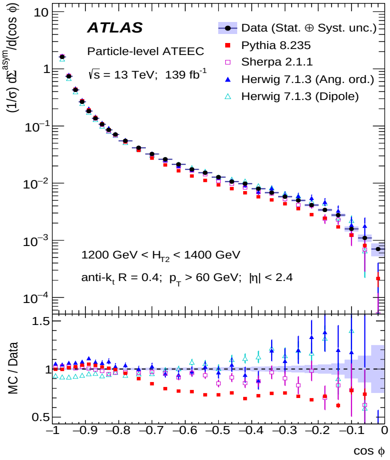

Transverse Energy-Energy Correlations in ATLAS [arXiv:2301.09351]

- Unfolding separately in each H_{T2} bin for computational reasons.
- Migrations over H_{T2} have a negligible impact on the results.
- Transfer matrix is highly diagonal (excellent detector resolution).

As for the other event shapes: $R_i = \sum_j \frac{\mathcal{E}_j}{\mathcal{P}_i} M_{ij} T_j$

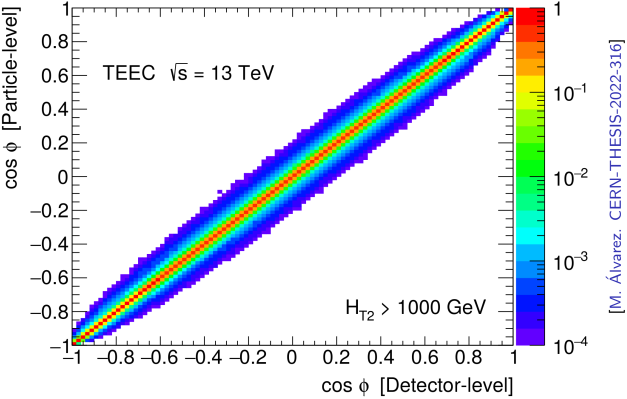

- Systematic uncertainties on jet energy (JES, JER) are dominant.
- Unfolding is performed with different Monte Carlo models.
- Uncertainties of $\mathcal{O}(2\% - 3\%)$ in central plateau, smaller for $\cos\phi \sim \pm 1$.
- Uncertainties on ATEEC are cancelled out to sub-percent level.

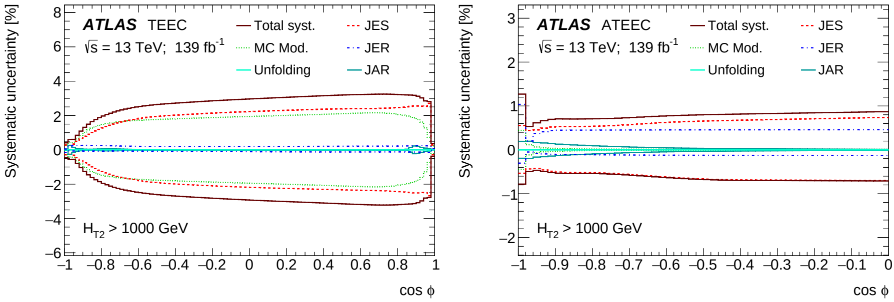

- Non-perturbative corrections obtained in different Pythia / Herwig tunes.
- Mostly unity, with some deviations observed in the collinear region.

$$C_{NP} = \left(\frac{1}{\sigma}\frac{d\Sigma}{d\cos\phi}\right)^{\mathrm{Had=ON}}_{\mathrm{UE=ON}} \Bigg/ \left(\frac{1}{\sigma}\frac{d\Sigma}{d\cos\phi}\right)^{\mathrm{Had=OFF}}_{\mathrm{UE=OFF}}$$

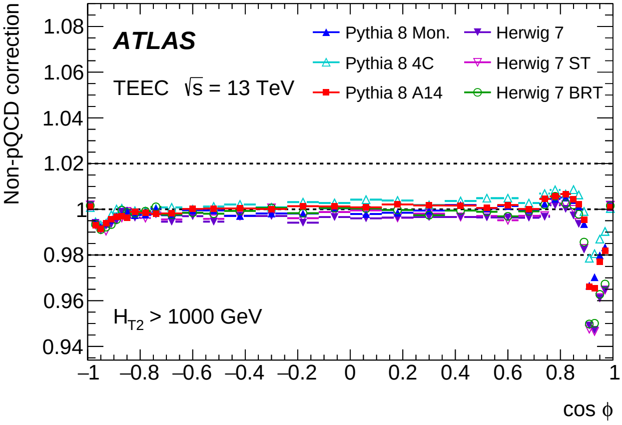

Transverse Energy-Energy Correlations in ATLAS [arXiv:2301.09351]

- Predictions avoid back-to-back and collinear regions $\Rightarrow |\cos\phi| < 0.92$.
- Theoretical uncertainties on the predictions are estimated on:
  - Renormalisation and factorisation scales μ_R, μ_F variations by a factor of 2.
  - Variations of the PDF parameters (eigenvectors / replicas).
  - Non-perturbative corrections with different MC tunes.
  - Variations of the strong coupling $\alpha_s(m_Z)$ by 0.0001.
- Total uncertainties of $\mathcal{O}(2\%)$ (3%) for TEEC (ATEEC).

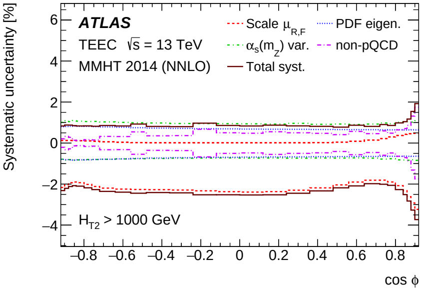

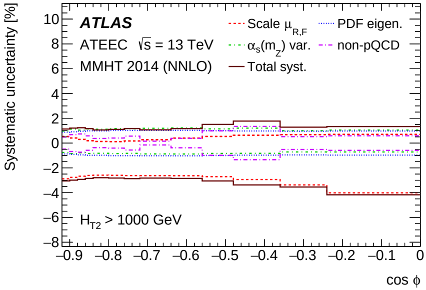

Transverse Energy-Energy Correlations in ATLAS [arXiv:2301.09351]

- Data are compared to theoretical predictions at LO, NLO and NNLO
- Intensive use of computing grid (**over 100M CPU hours $\sim$ 11K years!**)
- Excellent description of collinear and back-to-back regions.
- Important reduction of theoretical uncertainties on QCD scales.

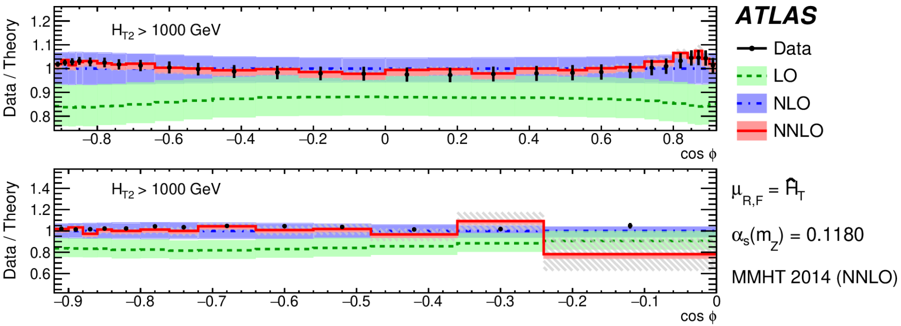

Good overall description, with theory slightly above the data for high H_{T2} bins.

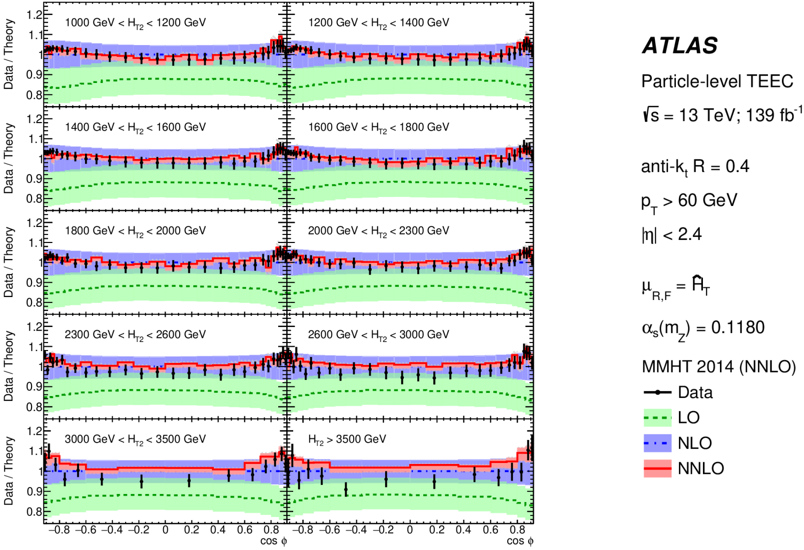

Good overall description, for ATEEC in all H_{T2} bins.

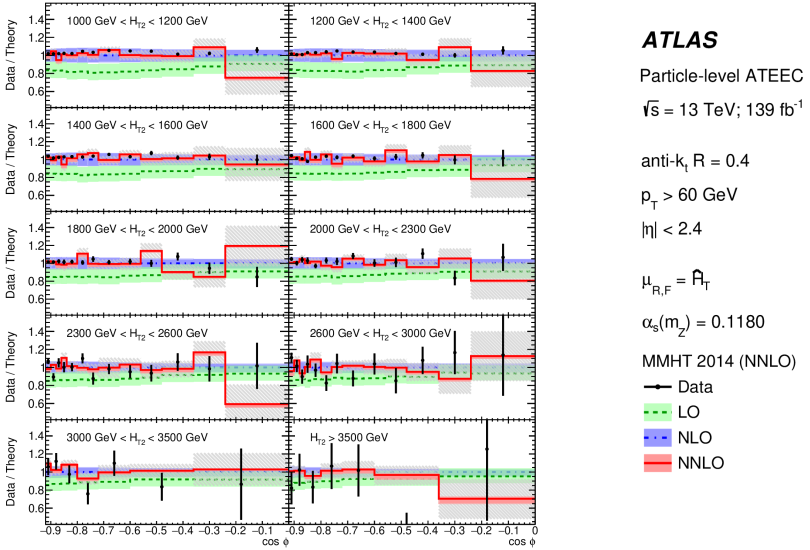

Transverse Energy-Energy Correlations in ATLAS [arXiv:2301.09351]

For determining $\alpha_s(m_Z)$, a χ^2 function is minimized in 149+1 dimensions

$$\left.\begin{aligned} \chi^2(\alpha_\mathrm{s}, \vec{\lambda}) &= \sum_{\mathrm{bins}} \frac{(x_i - F_i(\alpha_\mathrm{s}, \vec{\lambda}))^2}{\Delta x_i^2 + \Delta \xi_i^2} + \sum_k \lambda_k^2 \\ F_i(\alpha_\mathrm{s}, \vec{\lambda}) &= \psi_i(\alpha_\mathrm{s}) \left(1 + \sum_k \lambda_k \sigma_k^{(i)}\right) \end{aligned}\right\}$$

- x_i is the value of the data distribution in bin i.
- Δx_i and $\Delta \xi_i$ are the statistical uncertainties for data and theory.
- $\psi_i(\alpha_s) = \sum_{k=0}^{3} p_k^{(i)} \alpha_s^k$ parameterises the i-th bin dependence on $\alpha_s(m_Z)$.
- $\sigma_k^{(i)}$ are the relative experimental uncertainties (149 sources).
- λ_k are nuisance parameters for each experimental uncertainty.
- Scale uncertainties treated using the offset method: $\psi_i(\alpha_s)$ is varied.

Transverse Energy-Energy Correlations in ATLAS [arXiv:2301.09351]

Global TEEC fit uses information across the ten exclusive H_{T2} bins together

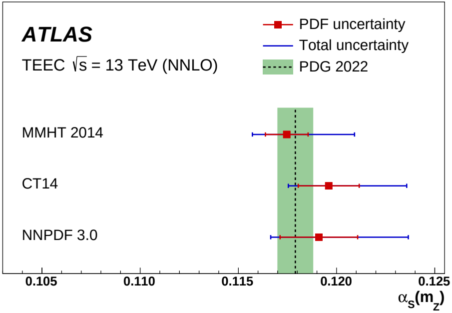

PDF	$\alpha_s(m_Z)$ value	$\chi^2/N_{\rm dof}$
MMHT 2014	0.1175 ± 0.0001 (stat.) ± 0.0006 (sys.)$^{+0.0032}_{-0.0011}$ (μ) ± 0.0011 (PDF) ± 0.0002 (NP) ± 0.0005 (mod.)	318 / 251
CT14	0.1196 ± 0.0001 (stat.) ± 0.0006 (sys.)$^{+0.0035}_{-0.0010}$ (μ) ± 0.0016 (PDF) ± 0.0002 (NP) ± 0.0006 (mod.)	262 / 251
NNPDF 3.0	0.1191 ± 0.0001 (stat.) ± 0.0006 (sys.)$^{+0.0040}_{-0.0011}$ (μ) ± 0.0020 (PDF) ± 0.0003 (NP) ± 0.0007(mod.)	300 / 251

Transverse Energy-Energy Correlations in ATLAS [arXiv:2301.09351]

Global ATEEC fit uses information across the ten exclusive H_{T2} bins together

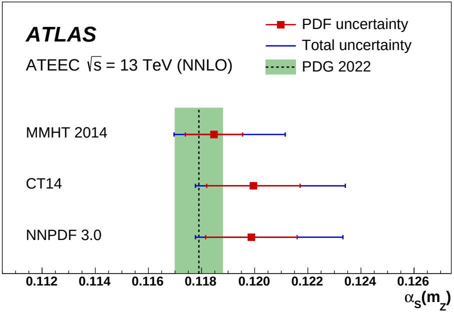

PDF	$\alpha_s(m_Z)$ value	χ^2/N_{dof}
MMHT 2014	0.1185 ± 0.0005 (stat.) ± 0.0008 (sys.)$^{+0.0022}_{-0.0002}$ (μ) ± 0.0011 (PDF) ± 0.0004 (NP) ± 0.0001 (mod.)	110 / 117
CT14	0.1200 ± 0.0006 (stat.) ± 0.0009 (sys.)$^{+0.0027}_{-0.0001}$ (μ) ± 0.0016 (PDF) ± 0.0005 (NP) ± 0.0001 (mod.)	110 / 117
NNPDF 3.0	$0.1199 \pm 0.0006 \pm$ (stat.)0.0009 (sys.)$^{+0.0027}_{-0.0002}$ (μ) ± 0.0017 (PDF) ± 0.0005 (NP) ± 0.0001(mod.)	108 / 117

Transverse Energy-Energy Correlations in ATLAS [arXiv:2301.09351]

- Values of $\alpha_s(m_Z)$ obtained from fits to TEEC functions on each bin
- For higher values of H_{T2}, the central values seem to go lower.
- Good χ^2 values for all H_{T2} regions considered.

$\langle \hat{H}_\mathrm{T} \rangle$ [GeV]	$\alpha_\mathrm{s}(m_Z)$ value (MMHT 2014)	χ^2/N_dof
Inclusive	0.1188 ± 0.0002 (stat.) ± 0.0007 (syst.) $^{+0.0030}_{-0.0002}$ (μ) ± 0.0010 (PDF) ± 0.0002 (NP) ± 0.0008 (mod.)	16.0 / 27
1302	0.1186 ± 0.0003 (stat.) ± 0.0009 (syst.) $^{+0.0031}_{-0.0001}$ (μ) ± 0.0010 (PDF) ± 0.0003 (NP) ± 0.0007 (mod.)	16.4 / 27
1518	0.1182 ± 0.0003 (stat.) ± 0.0009 (syst.) $^{+0.0027}_{-0.0005}$ (μ) ± 0.0010 (PDF) ± 0.0003 (NP) ± 0.0008 (mod.)	15.1 / 27
1732	0.1191 ± 0.0003 (stat.) ± 0.0011 (syst.) $^{+0.0030}_{-0.0005}$ (μ) ± 0.0011 (PDF) ± 0.0005 (NP) ± 0.0010 (mod.)	19.8 / 27
1944	0.1179 ± 0.0003 (stat.) ± 0.0011 (syst.) $^{+0.0030}_{-0.0005}$ (μ) ± 0.0011 (PDF) ± 0.0005 (NP) ± 0.0009 (mod.)	21.3 / 27
2153	0.1175 ± 0.0004 (stat.) ± 0.0012 (syst.) $^{+0.0029}_{-0.0004}$ (μ) ± 0.0011 (PDF) ± 0.0003 (NP) ± 0.0009 (mod.)	32.9 / 27
2396	0.1179 ± 0.0003 (stat.) ± 0.0012 (syst.) $^{+0.0029}_{-0.0005}$ (μ) ± 0.0012 (PDF) ± 0.0011 (NP) ± 0.0012 (mod.)	27.5 / 27
2706	0.1164 ± 0.0004 (stat.) ± 0.0015 (syst.) $^{+0.0030}_{-0.0005}$ (μ) ± 0.0013 (PDF) ± 0.0005 (NP) ± 0.0011 (mod.)	35.1 / 27
3042	0.1162 ± 0.0005 (stat.) ± 0.0017 (syst.) $^{+0.0031}_{-0.0005}$ (μ) ± 0.0013 (PDF) ± 0.0002 (NP) ± 0.0015 (mod.)	33.1 / 27
3476	0.1141 ± 0.0007 (stat.) ± 0.0017 (syst.) $^{+0.0033}_{-0.0011}$ (μ) ± 0.0014 (PDF) ± 0.0002 (NP) ± 0.0020 (mod.)	15.1 / 13
4189	0.1116 ± 0.0011 (stat.) ± 0.0018 (syst.) $^{+0.0030}_{-0.0009}$ (μ) ± 0.0015 (PDF) ± 0.0002 (NP) ± 0.0020 (mod.)	14.0 / 13

- Values of $\alpha_s(m_Z)$ obtained from fits to ATEEC functions on each bin
- For higher values of H_{T2}, the central values seem to go lower.
- Good χ^2 values for all H_{T2} regions considered.

$\langle \hat{H}_{\mathrm{T}} \rangle$ [GeV]	$\alpha_{\mathrm{s}}(m_Z)$ value (MMHT 2014)	χ^2/N_{dof}
Inclusive	0.1194 ± 0.0009 (stat.) ± 0.0007 (syst.) $^{+0.0023}_{-0.0000}$ (μ) ± 0.0011 (PDF) ± 0.0005 (NP) ± 0.0000 (mod.)	10.7 / 12
1302	0.1195 ± 0.0011 (stat.) ± 0.0006 (syst.) $^{+0.0024}_{-0.0000}$ (μ) ± 0.0011 (PDF) ± 0.0006 (NP) ± 0.0000 (mod.)	10.6 / 12
1518	0.1191 ± 0.0011 (stat.) ± 0.0007 (syst.) $^{+0.0020}_{-0.0001}$ (μ) ± 0.0011 (PDF) ± 0.0004 (NP) ± 0.0001 (mod.)	7.2 / 12
1732	0.1187 ± 0.0015 (stat.) ± 0.0009 (syst.) $^{+0.0026}_{-0.0003}$ (μ) ± 0.0012 (PDF) ± 0.0010 (NP) ± 0.0002 (mod.)	7.2 / 12
1944	0.1178 ± 0.0016 (stat.) ± 0.0009 (syst.) $^{+0.0022}_{-0.0001}$ (μ) ± 0.0013 (PDF) ± 0.0007 (NP) ± 0.0000 (mod.)	11.2 / 12
2153	0.1174 ± 0.0017 (stat.) ± 0.0009 (syst.) $^{+0.0022}_{-0.0002}$ (μ) ± 0.0013 (PDF) ± 0.0007 (NP) ± 0.0001 (mod.)	12.8 / 12
2396	0.1187 ± 0.0017 (stat.) ± 0.0010 (syst.) $^{+0.0017}_{-0.0000}$ (μ) ± 0.0012 (PDF) ± 0.0007 (NP) ± 0.0004 (mod.)	11.7 / 12
2706	0.1148 ± 0.0026 (stat.) ± 0.0014 (syst.) $^{+0.0024}_{-0.0001}$ (μ) ± 0.0015 (PDF) ± 0.0007 (NP) ± 0.0002 (mod.)	18.3 / 12
3042	0.1169 ± 0.0031 (stat.) ± 0.0012 (syst.) $^{+0.0018}_{-0.0000}$ (μ) ± 0.0015 (PDF) ± 0.0014 (NP) ± 0.0009 (mod.)	13.0 / 12
3476	0.1141 ± 0.0052 (stat.) ± 0.0016 (syst.) $^{+0.0025}_{-0.0007}$ (μ) ± 0.0018 (PDF) ± 0.0008 (NP) ± 0.0011 (mod.)	4.9 / 6
4189	0.1096 ± 0.0085 (stat.) ± 0.0009 (syst.) $^{+0.0013}_{-0.0000}$ (μ) ± 0.0009 (PDF) ± 0.0002 (NP) ± 0.0007 (mod.)	6.2 / 6

- The value of $\alpha_s(m_Z)$ is evolved to $\alpha_s(Q)$ for each H_{T2} bin using the RGE.
- The value $Q = \langle \hat{H}_T \rangle / 2$ is chosen for comparison with other analyses.
- $\langle \hat{H}_T \rangle$ is obtained for each H_{T2} bin using the NNLO predictions.

$$\frac{\alpha_s}{4\pi}(Q^2) = \frac{1}{\beta_0 x}\left[1 - \frac{\beta_1}{\beta_0^2}\frac{\log x}{x} + \frac{\beta_1^2}{\beta_0^4 x^2}\left(\log^2 x - \log x - 1 + \frac{\beta_2 \beta_0}{\beta_1^2}\right)\right]; \quad x = \log\left(\frac{Q^2}{\Lambda^2}\right)$$

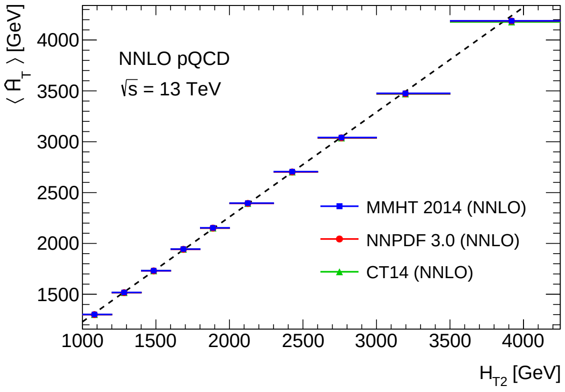

[M. Álvarez. CERN-THESIS-2022-316]

- Improves theory uncertainties by a factor of 3 with respect to NLO.
- Good agreement with world average and previous measurements.
- Renormalisation Group Equation probed at the highest scales to date.
- Provides the highest precision points beyond the TeV scale to date.

[ATLAS-CONF-2020-025] (NLO)

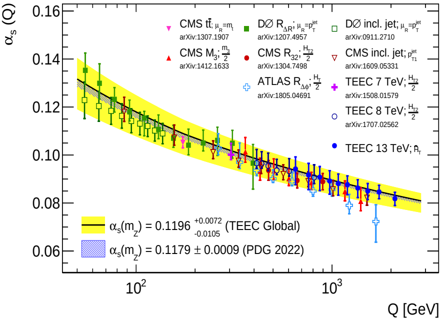

[arXiv:2301.09351] (NNLO)

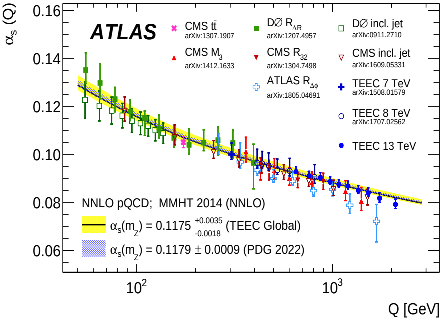

- Improves theory uncertainties by a factor of 3 with respect to NLO.
- Good agreement with world average and previous measurements.
- Renormalisation Group Equation probed at the highest scales to date.
- Provides the highest precision points beyond the TeV scale to date.

[ATLAS-CONF-2020-025] (NLO)

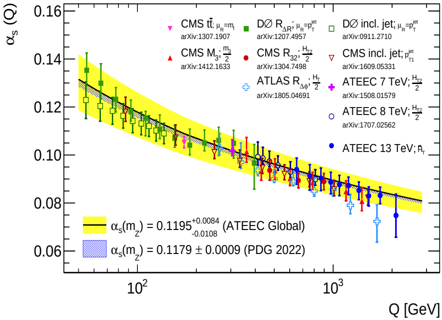

[arXiv:2301.09351] (NNLO)

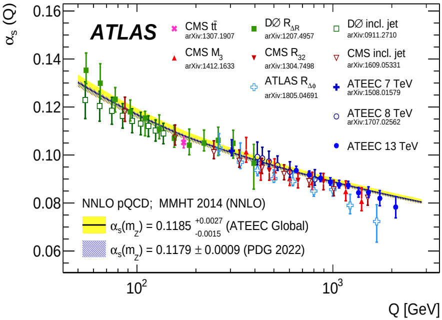

- The dependence on the PDF is studied in detail for $\alpha_s(Q)$.
- A small dependence, although noticeable, is observed on the PDF set.

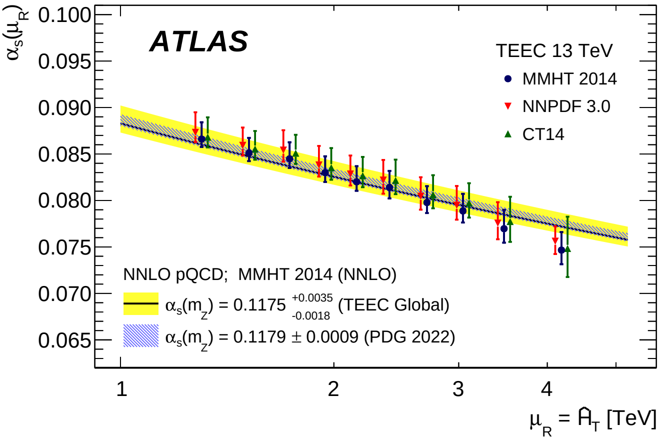

Transverse Energy-Energy Correlations in ATLAS [arXiv:2301.09351]

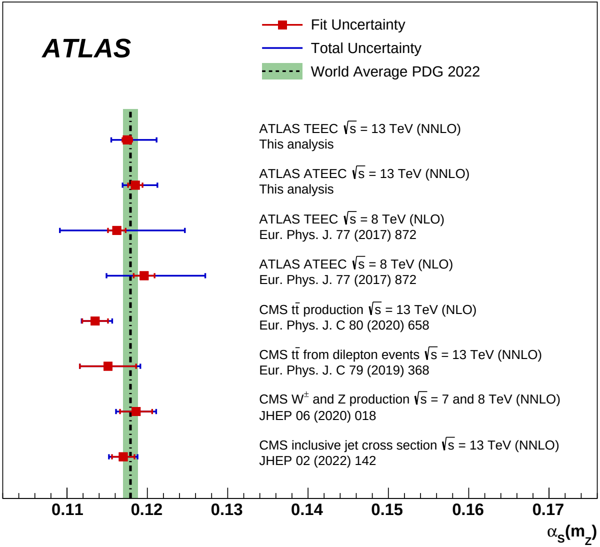

Using the QCD coupling to constrain new physics [NPB 936, 106 (2018)]

- Testing the running coupling is an important precision test of the SM.
- But also a way to study contributions from new physics beyond the SM!
- New coloured fermions would modify the structure of the β function.

Becciolini et al. [PRD 92, 079905 (2015)]; Llorente, Nachman [NPB 936, 106 (2018)]

Standard Model with n_f quark flavours + n_X

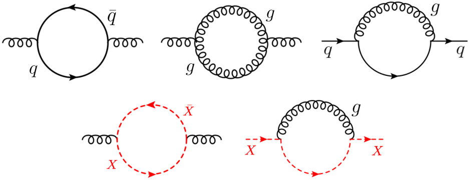

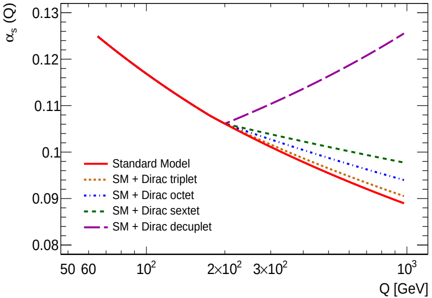

$$\left.\begin{aligned}\beta_0 &= 11 - \frac{2}{3}n_f - \frac{4}{3}n_X T_X \\ \beta_1 &= 102 - \frac{38}{3}n_f - 20 n_X T_X\left(1 + \frac{C_X}{5}\right)\end{aligned}\right\}$$

	Triplet	Octet	Sextet	Decuplet
T_X	1/2	3	5/2	15/2
C_X	4/3	3	10/3	6

Using the QCD coupling to constrain new physics [NPB 936, 106 (2018)]

- The TEEC and ATEEC are obtained over a range of m_X and T_X.
- The modifications on $\alpha_s(Q)$ translate into effects on the distributions.
- Modified (SM+X) distributions can be used to evaluate a p-value.

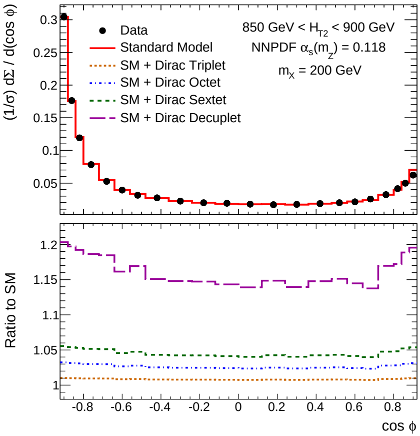

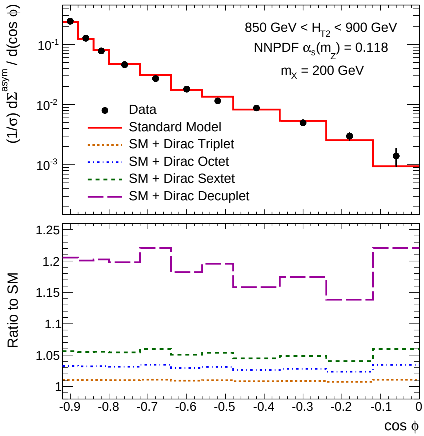

Using the QCD coupling to constrain new physics [NPB 936, 106 (2018)]

- A scan is performed over m_X and $n_{eff} = 2 n_X T_X$.
- Likelihood L is built using the covariance matrix V.

$$\log L(X, \theta) = -\frac{1}{2}(X-\theta)^T V^{-1} (X-\theta)$$

- Models with p-value below 0.05 are excluded.
- ATEEC has less statistical power than TEEC.

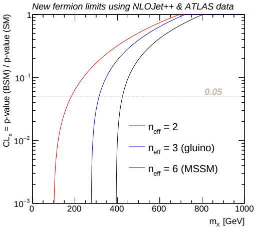

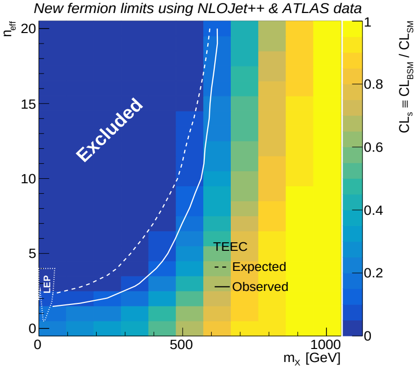

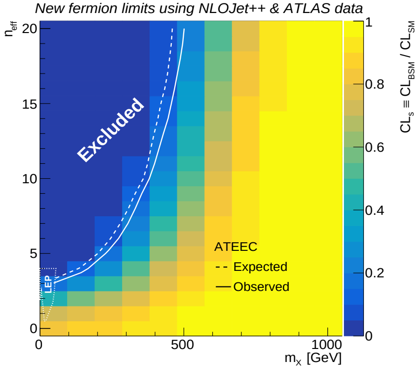

Summary and conclusions

- Event shapes are an interesting way to probe QCD at hadron colliders.
- Experimentally, three-jet event shapes are measured at $\mathcal{O}(1\%)$ precision.
- Recent theoretical progress allows for a more precise understanding;
  - Improved description of event shapes at the LHC
  - Reduced theoretical uncertainties on μ_R, μ_F.
- Experimentally, event shapes are measured with $\mathcal{O}(1\%)$ precision.
- This allows for precise determinations of $\alpha_s(m_Z)$ using TEEC.
- First comparisons of three-jet observables with NNLO predictions.
- Most precise determination of $\alpha_s(Q)$ over the TeV scale.
- This information can be used to set limits on new fermions beyond the SM.